Witnessing Nonequilibrium Entanglement Dynamics in a Strongly Correlated Fermionic Chain

Denitsa R. Baykusheva,[1*] Mona H. Kalthoff,[2] Damian Hofmann,[2] Martin Claassen,[3] Dante M. Kennes,[4,2] Michael A. Sentef,[2] and Matteo Mitrano[1†]

[1]*Department of Physics, Harvard University, Cambridge, Massachusetts 02138, USA*
[2]*Max Planck Institute for the Structure and Dynamics of Matter, Center for Free-Electron Laser Science (CFEL), Luruper Chaussee 149, 22761 Hamburg, Germany*
[3]*Department of Physics and Astronomy, University of Pennsylvania, Philadelphia, Pennsylvania 19104, USA*
[4]*Institut für Theorie der Statistischen Physik, RWTH Aachen University, 52056 Aachen, Germany and JARA-Fundamentals of Future Information Technology, 52056 Aachen, Germany*

(Received 21 August 2022; revised 13 January 2023; accepted 18 January 2023; published 6 March 2023)

Many-body entanglement in condensed matter systems can be diagnosed from equilibrium response functions through the use of entanglement witnesses and operator-specific quantum bounds. Here, we investigate the applicability of this approach for detecting entangled states in quantum systems driven out of equilibrium. We use a multipartite entanglement witness, the quantum Fisher information, to study the dynamics of a paradigmatic fermion chain undergoing a time-dependent change of the Coulomb interaction. Our results show that the quantum Fisher information is able to witness distinct signatures of multipartite entanglement both near and far from equilibrium that are robust against decoherence. We discuss implications of these findings for probing entanglement in light-driven quantum materials with time-resolved optical and x-ray scattering methods.

DOI: 10.1103/PhysRevLett.130.106902

Introduction.—A defining feature of quantum mechanics is the existence of nonlocal correlations and entanglement between distinct physical objects [1,2]. Entanglement is ubiquitous in the study of quantum many-body phenomena, encompassing areas such as quantum gravity [3], quantum information [4,5], and condensed matter physics [6–11]. Especially in the latter, entanglement has significant effects on the macroscopic behavior of quantum materials [12,13] and is intimately connected with the appearance of quantum spin liquidity [14–17], topological order [11,16], quantum criticality [18], and strange metallic behavior [19,20]. Therefore, efforts to identify and quantify quantum correlations in solids have the potential to reveal new collective phenomena and to advance our capability to harness their functionalities.

While small entangled systems can be experimentally characterized via tomography [21,22] or quantum interference methods [23], diagnosing entanglement in solids requires alternative approaches linked to accessible experimental observables [6,7,24]. A possible strategy relies on determining the expectation values of operators called "entanglement witnesses" [13,25–31]. The witness selection depends on the type of system and entanglement of interest, but a prominent quantity is the quantum Fisher information (QFI). At equilibrium, the QFI can be rigorously extracted from a sum-rule integral of the Kubo response function [32] and acts as a multipartite entanglement witness if its value exceeds classical expectations. Its connection with experimentally accessible response functions motivated recent inelastic neutron scattering studies of multipartite entanglement in a variety of spin chains [33–35] and defines a model-independent pathway to detect entangled states in quantum materials.

Witnessing entanglement with the QFI or other measures has significant implications well beyond the study of quantum systems at equilibrium. Recently, ultrafast laser pulses have enabled new pathways to drive quantum materials through nonequilibrium phase transitions, or induce entirely new states of matter without apparent equilibrium analogs [36–43]. Probing quantum entanglement for these dynamical phenomena is crucial in order to understand their microscopic origin and to identify the possible role of transient quantum coherence, especially in systems without obvious order parameters [44–47]. Hence, it becomes important to investigate how a time-dependent QFI reflects the evolution of entanglement through a nonequilibrium phase transition.

In this Letter, we show that the QFI is a robust witness of time-dependent multipartite entanglement across a prototypical nonequilibrium phase transition. We consider the experimentally relevant case of a fermion chain with a dynamically tuned Coulomb repulsion [48–51] and map its entanglement dynamics for different driving conditions. Upon ramping the interaction strength, the system undergoes a quantum phase transition from a disordered to an ordered phase. The QFI witnesses an increase in multipartite

 © 2023 American Physical Society

entanglement while ramping the Coulomb interaction. For adiabatic ramps, the QFI exhibits a well-defined local maximum at the critical point, consistent with expectations for equilibrium quantum phase transitions [32]. By contrast, in a diabatic regime its increase persists deep into the ordered phase with distinctive oscillatory behavior. Crucially, such enhancement is robust against the introduction of local decoherence processes, thus underscoring the possibility to witness entanglement dynamics of quantum systems coupled to realistic dissipative baths. Our results are immediately relevant to the nonequilibrium dynamics of one-dimensional Mott insulators in the strong coupling limit [e.g. $[\mathrm{Ni(chxn)_2Br}]\mathrm{Br_2}$, K-TCNQ, and (ET)-$\mathrm{F_2}$TCNQ] [48,52–57], and, through a mapping onto an equivalent spin model, of spin chain systems such as $\mathrm{Cs_2CoCl_4}$ [34], $\mathrm{KCuF_3}$ [35], or $[\mathrm{Cu}(\mu\text{-}\mathrm{C_2O_4})(4\text{-aminopyridine})_2(\mathrm{H_2O})]_n$ [33]. More broadly, our work defines a strategy to distinguish different dynamical regimes in driven materials via quantum information methods.

Model.—We consider a half-filled chain of spinless fermions interacting through a nearest-neighbor Coulomb repulsion. The model Hamiltonian reads:

$$\hat{\mathcal{H}}(t) = -\frac{J}{2}\sum_j (\hat{c}_j^\dagger \hat{c}_{j+1} + \mathrm{H.c.}) + V(t)\sum_j \tilde{n}_j \tilde{n}_{j+1}, \quad (1)$$

where $\hat{c}_j^\dagger$ ($\hat{c}_j$) is a creation (annihilation) operator at site j, $\tilde{n}_j = \hat{c}_j^\dagger \hat{c}_j - 1/2$ is the number operator relative to half filling, and J is a constant hopping amplitude setting the energy scale of our model. We consider a time-dependent nearest-neighbor Coulomb interaction $V(t)$, which can be realized in ultrafast optical experiments through dielectric screening enhancement [49], coherent Floquet dressing [43,58], or transient crystal lattice distortions [59]. For simplicity, we ramp up the interaction strength at constant velocity as $V(t) = Jvt$ for all the calculations presented in this Letter. At equilibrium, this system exhibits a well-known quantum phase transition at $V = 1$ from a gapless Luttinger liquid (LL) with short-range correlations to a charge density wave (CDW) with long-range correlations.

We map the spinless fermions onto an equivalent spin-1/2 anisotropic Heisenberg chain [Fig. 1(a)] via a Jordan-Wigner transformation [60,61] and add a small staggered magnetic field $h_z = 0.005$ (cf. Secs. S1 and S2 in the Supplemental Material [62]) in order to select one of the two classical Néel states. We have checked that our key results are robust against the specific value of the field. We study the nonequilibrium entanglement dynamics through exact diagonalization (ED) calculations using the QuSpin [64,65] and HPhi [66] packages. In the equivalent spin formulation, the quantum phase transition occurs between the XY and antiferromagnetic phases. Here, we report ED calculations for a 10-site spin chain with periodic boundary conditions (PBC) and benchmark a selected subset of these against real-time density matrix renormalization group

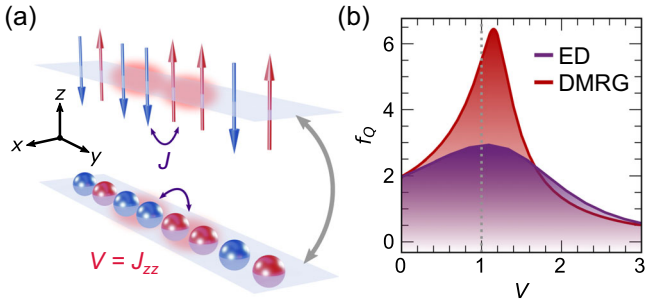

FIG. 1. (a) Sketch of half-filled spinless fermion chain with nearest-neighbor Coulomb interaction [Eq. (1)] (lower) and a corresponding spin-1/2 anisotropic Heisenberg model (upper). The fermionic hopping amplitude corresponds to the exchange coupling J and the Hubbard interaction V becomes the z-direction exchange coupling J_{zz}. (b) Equilibrium QFI density as a function of the intersite Coulomb repulsion V computed using ED for a $L = 10$ chain (purple) and using DMRG for an infinite chain (red), respectively. If $f_Q > 1$, the system is at least bipartite entangled.

(DMRG) calculations [67] on an infinite fermionic chain. ED calculations for chains of up to 24 sites (also with PBC) are included in the Supplemental Material [62].

We probe the entanglement dynamics by directly calculating the time-dependent QFI density using the instantaneous wave function describing the system. For a pure state ψ_0, the QFI associated with an operator $\hat{\mathcal{O}}_q$ is simply the connected correlation function [32]:

$$\mathcal{F}_Q = 4\Delta(\hat{\mathcal{O}}_q)^2 = 4(\langle\psi_0|\hat{\mathcal{O}}_q^2|\psi_0\rangle - \langle\psi_0|\hat{\mathcal{O}}_q|\psi_0\rangle^2). \quad (2)$$

Since we focus on phase transitions to states with staggered correlations at wave vector $q = \pi$ [60], we choose the local generator $\hat{\mathcal{O}}_\pi = \sum_l (-1)^l \hat{S}_l^z$ (formulated in the spin language). A value of the QFI density $f_Q \equiv \mathcal{F}_Q/L > m$, where m is a divisor of the system size L, signals that the state $|\psi_0\rangle$ must be $m+1$-partite entangled [30,32,68].

Results.—Owing to the superposition of an increasing number of states due to quantum fluctuations, a system approaching a nontopological quantum phase transition (i.e., one with a local order parameter on the quasi-ordered side of the phase transition) will exhibit enhanced multipartite entanglement and a QFI maximum around the critical point [32]. We first investigate the evolution of the QFI density f_Q upon tuning the interactions across the equilibrium critical point. As shown in Fig. 1(b), f_Q correctly identifies the quantum phase transition ($V = 1$) via a clear local maximum. This behavior is common to both the small and infinite-size limits (cf. Sec. S2 in [62]), whereby the chain length mainly determines the sharpness of the QFI maximum, with minor effects on its exact position. In the gapless (LL) phase, the QFI density exceeds the classical bound $f_Q = 1$, thus witnessing at least bipartite entanglement. In the gapped (CDW) regime, the QFI density becomes featureless and decreases below the

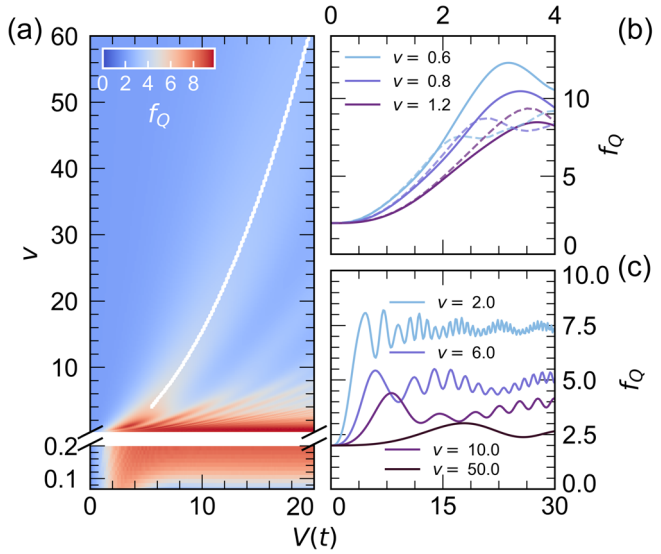

FIG. 2. (a) Nonequilibrium QFI density $f_Q = \mathcal{F}_Q/L$ as a function of the time-dependent interaction strength and ramp velocity for $L = 10$ sites. The white line marks the position of the instantaneous maxima of f_Q in the impulsive region (see text). The lower part of the panel is an enlargement of the quasi-adiabatic region. (b) Comparison between ED (dashed line) and DMRG (solid line) calculations of the time-dependent QFI density f_Q for selected ramp velocities. (c) Time-dependent QFI density f_Q for various ramp velocities.

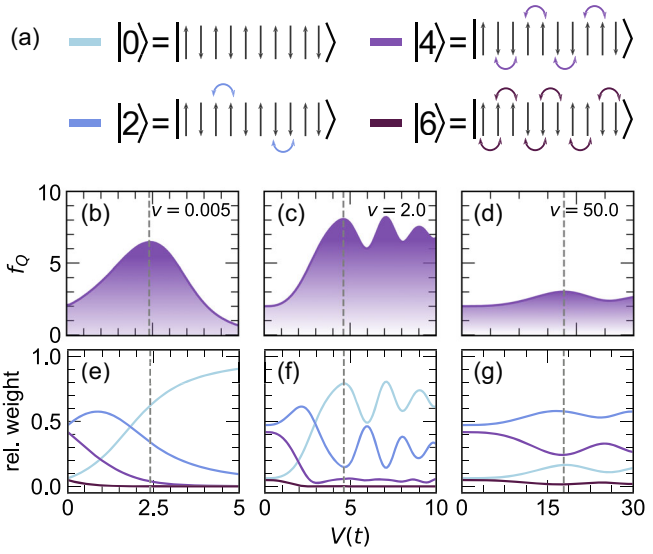

FIG. 3. Nonequilibrium QFI (top) and time-dependent density of defects (bottom) for selected velocities, (b),(e) $v = 0.005$, (c), (f) $v = 2$, and (d),(g) $v = 50$. Dashed vertical lines indicate the position of the first QFI maximum. (a) Chain configurations with a variable number of domain walls. The density of defects is given by the sum of the weights of time-evolved states containing zero to three domain walls. All calculations have been performed using the ED method.

classical bound, consistent with the absence of multipartite entanglement deep inside the ordered phase.

We now probe the nonequilibrium entanglement dynamics of our system. We consider a purely unitary evolution while ramping the interaction strength [see Fig. 2(a)]. Starting from the noninteracting limit, we calculate the QFI of the time-evolved initial state $|\psi_0(t)\rangle = \mathcal{T}\exp\left[-i\int_{t_0}^{t}\hat{\mathcal{H}}(t')\mathrm{d}t'\right]|\psi_0(t_0)\rangle$ for a fine mesh of ramp velocities. In the adiabatic limit ($v \to 0$) the QFI density still peaks around the equilibrium quantum critical point. However, its nonequilibrium behavior exhibits significant differences. Upon increasing ramp speed, the local QFI maximum undergoes a long-lived enhancement with no signs of decay at large interaction strength. The transition to a diabatic regime occurs at relatively low velocity through a highly entangled state with $f_Q \sim L$. By decomposing the eigenstates of the instantaneous Hamiltonian into Fock states specifying the spins at each lattice site, we see that the entanglement growth of this region is mainly driven by a "Schrödinger-cat"-like superposition of nearly degenerate Néel states $|\uparrow\downarrow\uparrow\downarrow\ldots\rangle$ and $|\downarrow\uparrow\downarrow\uparrow\ldots\rangle$ [69–82]. As we show later, this coherent superposition is not stable with respect to decoherence. At higher ramp velocity ($v > 3.5$), the nonequilibrium enhancement of the QFI density peaks at larger interaction strengths (earlier times) and at a progressively lower level, thus suggesting a lower degree of multipartite entanglement. Intriguingly, the existence of the main peak of the time-dependent QFI density does not depend on the system size [see Fig. 2(b)] while its position is insensitive to the presence of additional interaction terms in the equilibrium model (Sec. S6 in [62]). Hence, it represents a genuine nonequilibrium feature which does not extrapolate to the equilibrium critical point [83] and can be used to define a critical speed v^* separating adiabatic and diabatic ('impulsive') dynamical regimes. In addition, the QFI density enhancement is accompanied by a characteristic oscillatory behavior [see Fig. 2(c)]. These oscillations contain both size-dependent and size-independent frequency components, as analyzed in greater detail in Sec. S3 of the Supplemental Material [62]. Through a time-frequency analysis via a sliding-window Fourier transform, we assign these oscillations to transitions across the gap of the instantaneous Hamiltonian $\omega(t) \approx \Delta(t)$ [84,85].

To microscopically interpret the observed nonequilibrium entanglement dynamics, we decompose the instantaneous wavefunction $\psi_0(t)$ as a weighted superposition of Néel-like spin configurations with increasing number of domain walls (or *defects*, s. Fig. 3(a)). We then map the nonequilibrium QFI density at selected ramp velocities onto the time-dependent behavior of these weights (see Fig. 3). In the adiabatic limit ($v \lesssim 0.03$, see Fig. 3(b) and 3(f)), our system at $t_0 = 0$ is initialized in a disordered phase with a high density of defects. As the interaction strength grows, the time-evolved wavefunction $\psi_0(t)$ follows the ground state of the equilibrium Hamiltonian with effective interaction $V(t)$ and shows an increased superposition of pure Néel states without domain walls. Since the equally

weighted superposition of Néel states is maximally entangled and the underlying wave function cannot be represented as a product state, the QFI density f_Q increases to a value close to the system size ($f_Q \sim L$). Then, above the transition into the ordered phase, f_Q decays as the system selects one of the two Néel configurations and reduces the amount of multipartite entanglement.

At small ramp velocities [$0.175 < v < 3.5$, see Figs. 3(c) and 3(f)], the entanglement dynamics becomes diabatic and involves the excitation of states with nonzero defect density. The system still features a growth of the superposition between pure Néel configurations with the QFI density f_Q approaching the maximum value allowed by the system size. However, the departure from adiabaticity leads to the excitation of multiple low-lying states with a finite number of domain walls, their population being periodically redistributed as a function of time. At large ramp velocities [$v > 3.5$, see Figs. 3(d) and 3(g)], the QFI dynamics is deep in the diabatic regime. The time-evolved wave function does not follow the ground state evolution and its composition becomes skewed towards states with a nonzero number of domain walls. The superposition of pure Néel configurations is suppressed and the overall entanglement content of our model is reduced. In other words, a rapid change of the interaction strength drives the system into states with a larger number of defects and lower multipartite entanglement.

Since the QFI behavior is closely related to the proliferation of defects, we verify whether this entanglement witness follows a dynamics of the Kibble-Zurek (KZ) type [86,87]. In the KZ picture, the dynamics of a system undergoing a quantum phase transition, including the scaling of the density of defects and other observables as a function of the quench velocity, is determined by its behaviour at the critical point [88–90]. While the validity of the KZ mechanism in the quantum regime has been established for trajectories across a critical point, our quench from the disordered to the ordered phase requires crossing an entire critical region ($0 \leq \Delta < 1$) [91,92] and the critical point at $V = 1$ is of the Berezinskii-Kosterlitz-Thouless (BKT) type [93]. Figure 3 and the corresponding analysis strongly imply the existence of a tight connection between the extrema of the dynamical QFI and the number of defects as a function of time. In Fig. S6 of the Supplemental Material [62], we show that the maximum of $f_Q(t)$ in fact coincides with a minimum of the integrated density of defects, consistent with the fact that the predominance of the Néel-like configuration is conducive to higher entanglement levels. Therefore, in the following we interpret the scaling of the time instant t^* maximizing the dynamical QFI density f_Q in terms of the KZ paradigm. In the impulsive regime, we find that the nearest-neighbour Coulomb repulsion $V(t^*)$ maximizing the QFI density f_Q is consistent with the KZ expectation and follows a dynamical scaling given by the power law $V(t^*) \propto v^\alpha$ with $\alpha \approx 1/2$ (0.5295 ± 0.0009). In Sec. S5 of the Supplemental Material [62], we relate α with the critical exponent of the system and the scaling of the gap at the critical point $V = 1$. Remarkably, for the systems sizes investigated here the KZ scaling of $V(t^*)$ is insensitive to diverse microscopic perturbations of the equilibrium model such as second-neighbor interactions, decoherence, or external fields [62].

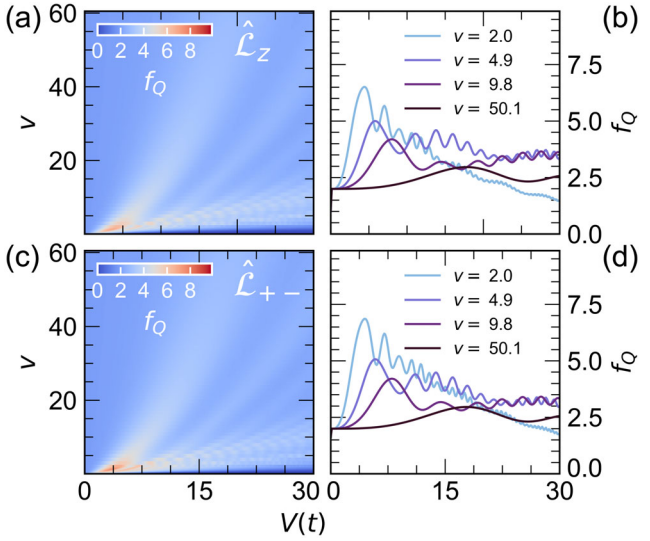

FIG. 4. Nonequilibrium QFI density $f_Q = \mathcal{F}_Q/L$ as a function of time and ramp velocity for $L = 10$ sites and at fixed decoherence rate $\gamma = 0.01$. (a),(c) Evolution of f_Q in the presence of the Lindbladian jump operators $\hat{\mathcal{L}}_z$ and $\hat{\mathcal{L}}_{+-}$, respectively. (b), (d) Time-dependent f_Q curves for selected ramp velocities. The calculations have been performed employing the ED method.

Since most nonequilibrium experiments on condensed matter systems involve the coupling to an external environment, we now verify that the QFI density enhancement survives the presence of quantum dissipation. We evolve the density matrix $\hat{\rho}(t) = |\psi_0(t)\rangle\langle\psi_0(t)|$ according to a Lindblad master equation with a decoherence rate γ

$$\dot{\hat{\rho}}(t) = -i[\hat{\mathcal{H}}(t), \hat{\rho}(t)] + 2\gamma \sum_{l=0}^{L-1} \left(\hat{\mathcal{L}}_l \hat{\rho}(t) \hat{\mathcal{L}}_l^\dagger - \frac{1}{2}\{\hat{\mathcal{L}}_l^\dagger \hat{\mathcal{L}}_l, \hat{\rho}(t)\} \right). \tag{3}$$

We choose two different quantum jump operators $\hat{\mathcal{L}}_l$, namely $\hat{\mathcal{L}}_z \equiv \hat{\sigma}_l^z$ and $\hat{\mathcal{L}}_{+-} \equiv \hat{\sigma}_l^+ \hat{\sigma}_{l+1}^-$. The former describes local dephasing, relevant to the description of decay processes involving local degrees of freedom, such as molecular vibrations [55]. The latter encodes instead nonlocal quantum decoherence [94] relevant to systems featuring magneto-elastic coupling where the spin-exchange process is coupled to a bath of vibrational oscillators. The calculation of the QFI in this case follows the definition for a mixed state

$$\mathcal{F}_Q(t) = 2 \sum_{i,j} \frac{(\epsilon_t^i - \epsilon_t^j)^2}{\epsilon_t^i + \epsilon_t^j} |\langle \varphi_t^i | \hat{\mathcal{O}}_\pi | \varphi_t^j \rangle|^2, \tag{4}$$

where ϵ_t^i and $|\varphi_t^i\rangle$ are eigenvalues and eigenvectors of $\hat{\rho}$ at time t (see Sec. S4 in the Supplemental Material [62] for further details). As shown in Fig. 4, the decoherence terms suppress the Schrödinger-cat-like state at low ramp speeds and introduce a decay of the QFI density for increasing interaction strength. However, the main nonequilibrium QFI peak is preserved and persists up to coupling rates of $\gamma \approx 0.1$ [62] with only minor changes in location and magnitude. A decoherence rate $\gamma = 0.1$ is consistent with the experimental quasiparticle recombination rates of certain quasi-1D Mott insulators [55]. Hence, it should be possible to use the QFI density to witness nonequilibrium entanglement dynamics in realistic quantum systems subject to decoherence.

Conclusion.—We have investigated the nonequilibrium evolution of a driven fermion chain in terms of its many-body entanglement properties. By dynamically tuning the intersite Coulomb repulsion, we witness the multipartite entanglement dynamics with the time-dependent QFI across a prototypical quantum phase transition and find it robust against the introduction of decoherence.

The existence of a rigorous connection between the QFI and the dynamical response of quantum systems at equilibrium has motivated recent attempts to witness multipartite entanglement in inelastic neutron scattering experiments [33–35]. The same protocols could be extended to certify the presence of entangled states in driven systems with ultrafast resonant inelastic x-ray scattering and optical methods. Our Letter establishes the QFI as a valid nonequilibrium entanglement witness for driven condensed matter systems beyond its current use in quantum simulators and quantum information science [95–100]. However, further progress in this direction requires mapping the QFI operator to transient response functions (thus abandoning the fluctuation-dissipation theorem as the key tenet of Ref. [32]), determining appropriate quantum bounds for the relevant observables, and controlling sources of experimental uncertainties (e.g. energy resolution broadening or incorrect normalization of experimental spectra) which could lead to an inaccurate extraction of the QFI [32,34,35]. These steps will extend the use of entanglement witnesses to future nonequilibrium spectroscopy experiments on quantum materials.

Our findings pave the way towards a deeper understanding of the role of quantum correlations in photoinduced phase transitions. The entanglement dynamics studied here is immediately relevant to laser-driven quasi-one-dimensional Mott insulators and spin chain materials [67] and represents a template to understand the more general behavior of correlated quantum materials out of equilibrium. In particular, entanglement correlations might allow for a better characterization of hitherto incompletely understood pathways towards hidden metastable phases [47,101], the identification of dynamical quantum phases without obvious order parameters [102,103], and could be key in unraveling the mystery behind light-induced phases of matter without equilibrium analogs [104].

We would like to thank S. R. Clark, J. Marino, Y. Wang, N. Yao, and P. Zoller for insightful discussions. This work was primarily supported by the U.S. Department of Energy, Office of Basic Energy Sciences, Early Career Award Program, under Award No. DE-SC0022883. M. M. further acknowledges support by the Aramont Fellowship Fund for Emerging Science Research at Harvard University. D. R. B. was supported by the Swiss National Science Foundation through Project No. P400P2_194343. M. C. acknowledges support by NSF Grant No. DMR-2132591. D. M. K. acknowledges funding by the Deutsche Forschungsgemeinschaft (DFG, German Research Foundation) via Germany's Excellence Strategy—Cluster of Excellence Matter and Light for Quantum Computing (ML4Q) EXC 2004/1—390534769 and within the RTG 1995. M. A. S. acknowledges financial support through the Deutsche Forschungsgemeinschaft (DFG, German Research Foundation) via the Emmy Noether program (SE 2558/2). We also acknowledge support from the Max Planck-New York City Center for Non-Equilibrium Quantum Phenomena.

*Corresponding author.
dbaykusheva@g.harvard.edu
†Corresponding author.
mmitrano@fas.harvard.edu

[1] J. S. Bell, *Speakable and Unspeakable in Quantum Mechanics. Collected Papers on quantum Philosophy* (Cambridge University Press, Cambridge, England, 1987).
[2] R. Horodecki, P. Horodecki, M. Horodecki, and K. Horodecki, Quantum entanglement, Rev. Mod. Phys. **81**, 865 (2009).
[3] T. Nishioka, S. Ryu, and T. Takayanagi, Holographic entanglement entropy: An overview, J. Phys. A **42**, 504008 (2009).
[4] D. Bouwmeester, A. Ekert, and A. Zeilinger, *The Physics of Quantum Information* (Springer, New York, 2000).
[5] M. A. Nielsen and I. L. Chuang, *Quantum Computation and Quantum Information* (Cambridge University Press, Cambridge, England, 2010).
[6] L. Amico, R. Fazio, A. Osterloh, and V. Vedral, Entanglement in many-body systems, Rev. Mod. Phys. **80**, 517 (2008).
[7] V. Vedral, Quantifying entanglement in macroscopic systems, Nature (London) **453**, 1004 (2008).
[8] N. Laflorencie, Quantum entanglement in condensed matter systems, Phys. Rep. **646**, 1 (2016).
[9] C. Gogolin and J. Eisert, Equilibration, thermalisation, and the emergence of statistical mechanics in closed quantum systems, Rep. Prog. Phys. **79**, 056001 (2016).
[10] M. Ueda, Quantum equilibration, thermalization and prethermalization in ultracold atoms, Nat. Rev. Phys. **2**, 669 (2020).
[11] B. Zeng, X. Chen, D.-L. Zhou, and X.-G. Wen, *Quantum Information Meets Quantum Matter—From Quantum Entanglement to Topological Phase in Many-Body Systems* (Springer, New York, NY, 2019).

[12] S. Ghosh, T. F. Rosenbaum, G. Aeppli, and S. N. Coppersmith, Entangled quantum state of magnetic dipoles, Nature (London) **425**, 48 (2003).

[13] Č. Brukner, V. Vedral, and A. Zeilinger, Crucial role of quantum entanglement in bulk properties of solids, Phys. Rev. A **73**, 012110 (2006).

[14] L. Balents, Spin liquids in frustrated magnets, Nature (London) **464**, 199 (2010).

[15] L. Savary and L. Balents, Quantum spin liquids: A review, Rep. Prog. Phys. **80**, 016502 (2016).

[16] X.-G. Wen, Colloquium: Zoo of quantum-topological phases of matter, Rev. Mod. Phys. **89**, 041004 (2017).

[17] G. Semeghini, H. Levine, A. Keesling, S. Ebadi, T. T. Wang, D. Bluvstein, R. Verresen, H. Pichler, M. Kalinowski, R. Samajdar, A. Omran, S. Sachdev, A. Vishwanath, M. Greiner, V. Vuletić, and M. D. Lukin, Probing topological spin liquids on a programmable quantum simulator, Science **374**, 1242 (2021).

[18] L. Prochaska, X. Li, D. C. MacFarland, A. M. Andrews, M. Bonta, E. F. Bianco, S. Yazdi, W. Schrenk, H. Detz, A. Limbeck, Q. Si, E. Ringe, G. Strasser, J. Kono, and S. Paschen, Singular charge fluctuations at a magnetic quantum critical point, Science **367**, 285 (2020).

[19] J. Zaanen, Planckian dissipation, minimal viscosity and the transport in cuprate strange metals, SciPost Phys. **6**, 61 (2019).

[20] S.-D. Chen, M. Hashimoto, Y. He, D. Song, K.-J. Xu, J.-F. He, T. P. Devereaux, H. Eisaki, D.-H. Lu, J. Zaanen, and Z.-X. Shen, Incoherent strange metal sharply bounded by a critical doping in Bi2212, Science **366**, 1099 (2019).

[21] D. F. V. James, P. G. Kwiat, W. J. Munro, and A. G. White, Measurement of qubits, Phys. Rev. A **64**, 052312 (2001).

[22] H. Häffner, W. Hänsel, C. F. Roos, J. Benhelm, D. Chek-al kar, M. Chwalla, T. Körber, U. D. Rapol, M. Riebe, P. O. Schmidt, C. Becher, O. Gühne, W. Dür, and R. Blatt, Scalable multiparticle entanglement of trapped ions, Nature (London) **438**, 643 (2005).

[23] R. Islam, R. Ma, P. M. Preiss, M. Eric Tai, A. Lukin, M. Rispoli, and M. Greiner, Measuring entanglement entropy in a quantum many-body system, Nature (London) **528**, 77 (2015).

[24] O. Gühne and G. Tóth, Entanglement detection, Phys. Rep. **474**, 1 (2009).

[25] V. Coffman, J. Kundu, and W. K. Wootters, Distributed entanglement, Phys. Rev. A **61**, 052306 (2000).

[26] L. Amico, A. Osterloh, F. Plastina, R. Fazio, and G. Massimo Palma, Dynamics of entanglement in one-dimensional spin systems, Phys. Rev. A **69**, 022304 (2004).

[27] T. Roscilde, P. Verrucchi, A. Fubini, S. Haas, and V. Tognetti, Studying Quantum Spin Systems through Entanglement Estimators, Phys. Rev. Lett. **93**, 167203 (2004).

[28] L. Amico, F. Baroni, A. Fubini, D. Patanè, V. Tognetti, and P. Verrucchi, Divergence of the entanglement range in low-dimensional quantum systems, Phys. Rev. A **74**, 022322 (2006).

[29] L. Pezzé and A. Smerzi, Entanglement, Nonlinear Dynamics, and the Heisenberg Limit, Phys. Rev. Lett. **102**, 100401 (2009).

[30] P. Hyllus, W. Laskowski, R. Krischek, C. Schwemmer, W. Wieczorek, H. Weinfurter, L. Pezzé, and A. Smerzi, Fisher information and multiparticle entanglement, Phys. Rev. A **85**, 022321 (2012).

[31] G. Tóth and I. Apellaniz, Quantum metrology from a quantum information science perspective, J. Phys. A **47**, 424006 (2014).

[32] P. Hauke, M. Heyl, L. Tagliacozzo, and P. Zoller, Measuring multipartite entanglement through dynamic susceptibilities, Nat. Phys. **12**, 778 (2016).

[33] G. Mathew, S. L. L. Silva, A. Jain, A. Mohan, D. T. Adroja, V. G. Sakai, C. V. Tomy, A. Banerjee, R. Goreti, V. N. Aswathi, R. Singh, and D. Jaiswal-Nagar, Experimental realization of multipartite entanglement via quantum Fisher information in a uniform antiferromagnetic quantum spin chain, Phys. Rev. Res. **2**, 043329 (2020).

[34] P. Laurell, A. Scheie, C. J. Mukherjee, M. M. Koza, M. Enderle, Z. Tylczynski, S. Okamoto, R. Coldea, D. A. Tennant, and G. Alvarez, Quantifying and Controlling Entanglement in the Quantum Magnet Cs_2CoCl_4, Phys. Rev. Lett. **127**, 037201 (2021).

[35] A. Scheie, P. Laurell, A. M. Samarakoon, B. Lake, S. E. Nagler, G. E. Granroth, S. Okamoto, G. Alvarez, and D. A. Tennant, Witnessing entanglement in quantum magnets using neutron scattering, Phys. Rev. B **103**, 224434 (2021).

[36] W. Hu, S. Kaiser, D. Nicoletti, C. R. Hunt, I. Gierz, M. C. Hoffmann, M. Le Tacon, T. Loew, B. Keimer, and A. Cavalleri, Optically enhanced coherent transport in $YBa_2Cu_3O_{6.5}$ by ultrafast redistribution of interlayer coupling, Nat. Mater. **13**, 705 (2014).

[37] S. Kaiser, C. R. Hunt, D. Nicoletti, W. Hu, I. Gierz, H. Y. Liu, M. Le Tacon, T. Loew, D. Haug, B. Keimer, and A. Cavalleri, Optically induced coherent transport far above T_c in underdoped $YBa_2Cu_3O_{6+\delta}$, Phys. Rev. B **89**, 184516 (2014).

[38] M. Mitrano, A. Cantaluppi, D. Nicoletti, S. Kaiser, A. Perucchi, S. Lupi, P. Di Pietro, D. Pontiroli, M. Riccò, S. R. Clark, D. Jaksch, and A. Cavalleri, Possible light-induced superconductivity in K_3C_{60} at high temperature, Nature (London) **530**, 461 (2016).

[39] M. Buzzi *et al.*, Photomolecular High-Temperature Superconductivity, Phys. Rev. X **10**, 031028 (2020).

[40] Y. H. Wang, H. Steinberg, P. Jarillo-Herrero, and N. Gedik, Observation of Floquet-Bloch states on the surface of a topological insulator, Science **342**, 453 (2013).

[41] F. Mahmood, C.-K. Chan, Z. Alpichshev, D. Gardner, Y. Lee, P. A. Lee, and N. Gedik, Selective scattering between Floquet–Bloch and Volkov states in a topological insulator, Nat. Phys. **12**, 306 (2016).

[42] J. W. McIver, B. Schulte, F. U. Stein, T. Matsuyama, G. Jotzu, G. Meier, and A. Cavalleri, Light-induced anomalous Hall effect in graphene, Nat. Phys. **16**, 38 (2020).

[43] A. de la Torre, D. M. Kennes, M. Claassen, S. Gerber, J. W. McIver, and M. A. Sentef, Colloquium: Nonthermal pathways to ultrafast control in quantum materials, Rev. Mod. Phys. **93**, 041002 (2021).

[44] M. Claassen, H.-C. Jiang, B. Moritz, and T. P. Devereaux, Dynamical time-reversal symmetry breaking and photo-induced chiral spin liquids in frustrated Mott insulators, Nat. Commun. **8**, 1192 (2017).

[45] T. Kaneko, T. Shirakawa, S. Sorella, and S. Yunoki, Photoinduced η-Pairing in the Hubbard Model, Phys. Rev. Lett. **122**, 077002 (2019).
[46] F. Peronaci, O. Parcollet, and M. Schiró, Enhancement of local pairing correlations in periodically driven Mott insulators, Phys. Rev. B **101**, 161101(R) (2020).
[47] J. Li, D. Golez, P. Werner, and M. Eckstein, η-paired superconducting hidden phase in photodoped Mott insulators, Phys. Rev. B **102**, 165136 (2020).
[48] R. Singla, G. Cotugno, S. Kaiser, M. Först, M. Mitrano, H. Y. Liu, A. Cartella, C. Manzoni, H. Okamoto, T. Hasegawa, S. R. Clark, D. Jaksch, and A. Cavalleri, THz-Frequency Modulation of the Hubbard U in an Organic Mott Insulator, Phys. Rev. Lett. **115**, 187401 (2015).
[49] N. Tancogne-Dejean, M. A. Sentef, and A. Rubio, Ultrafast Modification of Hubbard U in a Strongly Correlated Material: Ab initio High-Harmonic Generation in NiO, Phys. Rev. Lett. **121**, 097402 (2018).
[50] S. Beaulieu, S. Dong, N. Tancogne-Dejean, M. Dendzik, T. Pincelli, J. Maklar, R. P. Xian, M. A. Sentef, M. Wolf, A. Rubio, L. Rettig, and R. Ernstorfer, Ultrafast dynamical Lifshitz transition, Sci. Adv. **7**, eabd9275 (2021).
[51] D. R. Baykusheva, H. Jang, A. A. Husain, S. Lee, S. F. R. TenHuisen, P. Zhou, S. Park, H. Kim, J.-K. Kim, H.-D. Kim, M. Kim, S.-Y. Park, P. Abbamonte, B. J. Kim, G. D. Gu, Y. Wang, and M. Mitrano, Ultrafast Renormalization of the On-Site Coulomb Repulsion in a Cuprate Superconductor, Phys. Rev. X **12**, 011013 (2022).
[52] S. Iwai, M. Ono, A. Maeda, H. Matsuzaki, H. Kishida, H. Okamoto, and Y. Tokura, Ultrafast Optical Switching to a Metallic State by Photoinduced Mott Transition in a Halogen-Bridged Nickel-Chain Compound, Phys. Rev. Lett. **91**, 057401 (2003).
[53] H. Okamoto, H. Matsuzaki, T. Wakabayashi, Y. Takahashi, and T. Hasegawa, Photoinduced Metallic State Mediated by Spin-Charge Separation in a One-Dimensional Organic Mott Insulator, Phys. Rev. Lett. **98**, 037401 (2007).
[54] H. Uemura, H. Matsuzaki, Y. Takahashi, T. Hasegawa, and H. Okamoto, Ultrafast charge dynamics in one-dimensional organic Mott insulators, J. Phys. Soc. Jpn. **77**, 113714 (2008).
[55] M. Mitrano, G. Cotugno, S. R. Clark, R. Singla, S. Kaiser, J. Stähler, R. Beyer, M. Dressel, L. Baldassarre, D. Nicoletti, A. Perucchi, T. Hasegawa, H. Okamoto, D. Jaksch, and A. Cavalleri, Pressure-Dependent Relaxation in the Photoexcited Mott Insulator $ET-F_2TCNQ$: Influence of Hopping and Correlations on Quasiparticle Recombination Rates, Phys. Rev. Lett. **112**, 117801 (2014).
[56] S. Wall, D. Brida, S. R. Clark, H. P. Ehrke, D. Jaksch, A. Ardavan, S. Bonora, H. Uemura, Y. Takahashi, T. Hasegawa, H. Okamoto, G. Cerullo, and A. Cavalleri, Quantum interference between charge excitation paths in a solid-state Mott insulator, Nat. Phys. **7**, 114 (2011).
[57] N. Sono, T. Otaki, T. Kitao, T. Yamakawa, D. Sakai, T. Morimoto, T. Miyamoto, and H. Okamoto, Phonon-dressed states in an organic Mott insulator, Commun. Phys. **5**, 72 (2022).
[58] J. H. Mentink, K. Balzer, and M. Eckstein, Ultrafast and reversible control of the exchange interaction in Mott insulators, Nat. Commun. **6**, 6708 (2015).
[59] A. S. Disa, T. F. Nova, and A. Cavalleri, Engineering crystal structures with light, Nat. Phys. **17**, 1087 (2021).
[60] T. Giamarchi, *Quantum Physics in One Dimension*, International Series of Monographs on Physics (Clarendon Press, Oxford, 2004).
[61] A. Altland and B. D. Simons, *Condensed Matter Field Theory* (Cambridge University Press, Cambridge, England, 2010).
[62] See Supplemental Material at http://link.aps.org/supplemental/10.1103/PhysRevLett.130.106902 for details on finite size effects, time-frequency, and Kibble-Zurek analysis of the nonequilibrium QFI, and for additional details about the Lindbladian evolution, which include Ref. [63].
[63] K. Patrick, V. Caudrelier, Z. Papić, and J. K. Pachos, Interaction distance in the extended XXZ model, Phys. Rev. B **100**, 235128 (2019).
[64] P. Weinberg and M. Bukov, QuSpin: A Python package for dynamics and exact diagonalisation of quantum many body systems. Part I: Spin chains, SciPost Phys. **2**, 003 (2017).
[65] P. Weinberg and M. Bukov, QuSpin: A Python package for dynamics and exact diagonalisation of quantum many body systems. Part II: Bosons, fermions and higher spins, SciPost Phys. **7**, 020 (2019).
[66] M. Kawamura, K. Yoshimi, T. Misawa, Y. Yamaji, S. Todo, and N. Kawashima, Quantum lattice model solver $\mathcal{H}\Phi$, Comput. Phys. Commun. **217**, 180 (2017).
[67] D. M. Kennes, A. de la Torre, A. Ron, D. Hsieh, and A. J. Millis, Floquet Engineering in Quantum Chains, Phys. Rev. Lett. **120**, 127601 (2018).
[68] G. Tóth, Multipartite entanglement and high-precision metrology, Phys. Rev. A **85**, 022322 (2012).
[69] D. M. Greenberger, M. A. Horne, and A. Zeilinger, Going beyond Bell's theorem, in *Bell's Theorem, Quantum Theory and Conceptions of the Universe*, edited by M. Kafatos (Springer Netherlands, Dordrecht, 1989), pp. 69–72.
[70] L. Pezzè, A. Smerzi, M. K. Oberthaler, R. Schmied, and P. Treutlein, Quantum metrology with nonclassical states of atomic ensembles, Rev. Mod. Phys. **90**, 035005 (2018).
[71] A. Ekert, R. Jozsa, R. Penrose, R. Laflamme, E. Knill, W. H. Zurek, P. Catasti, and S. V. S. Mariappan, NMR Greenberger-Horne-Zeilinger states, Phil. Trans. R. Soc. A **356**, 1941 (1998).
[72] P. Neumann, N. Mizuochi, F. Rempp, P. Hemmer, H. Watanabe, S. Yamasaki, V. Jacques, T. Gaebel, F. Jelezko, and J. Wrachtrup, Multipartite entanglement among single spins in diamond, Science **320**, 1326 (2008).
[73] D. Bouwmeester, J.-W. Pan, M. Daniell, H. Weinfurter, and A. Zeilinger, Observation of Three-Photon Greenberger-Horne-Zeilinger Entanglement, Phys. Rev. Lett. **82**, 1345 (1999).
[74] J.-W. Pan, M. Daniell, S. Gasparoni, G. Weihs, and A. Zeilinger, Experimental Demonstration of Four-Photon Entanglement and High-Fidelity Teleportation, Phys. Rev. Lett. **86**, 4435 (2001).

[75] X.-L. Wang, Y.-H. Luo, H.-L. Huang, M.-C. Chen, Z.-E. Su, C. Liu, C. Chen, W. Li, Y.-Q. Fang, X. Jiang, J. Zhang, L. Li, N.-L. Liu, C.-Y. Lu, and J.-W. Pan, 18-Qubit Entanglement With Six Photons' Three Degrees of Freedom, Phys. Rev. Lett. **120**, 260502 (2018).

[76] D. Leibfried, E. Knill, S. Seidelin, J. Britton, R. B. Blakestad, J. Chiaverini, D. B. Hume, W. M. Itano, J. D. Jost, C. Langer, R. Ozeri, R. Reichle, and D. J. Wineland, Creation of a six-atom "Schrödinger cat" state, Nature (London) **438**, 639 (2005).

[77] T. Monz, P. Schindler, J. T. Barreiro, M. Chwalla, D. Nigg, W. A. Coish, M. Harlander, W. Hänsel, M. Hennrich, and R. Blatt, 14-Qubit Entanglement: Creation and Coherence, Phys. Rev. Lett. **106**, 130506 (2011).

[78] N. Friis, O. Marty, C. Maier, C. Hempel, M. Holzäpfel, P. Jurcevic, M. B. Plenio, M. Huber, C. Roos, R. Blatt, and B. Lanyon, Observation of Entangled States of a Fully Controlled 20-Qubit System, Phys. Rev. X **8**, 021012 (2018).

[79] L. DiCarlo, M. D. Reed, L. Sun, B. R. Johnson, J. M. Chow, J. M. Gambetta, L. Frunzio, S. M. Girvin, M. H. Devoret, and R. J. Schoelkopf, Preparation and measurement of three-qubit entanglement in a superconducting circuit, Nature (London) **467**, 574 (2010).

[80] C. Song, K. Xu, W. Liu, C.-p. Yang, S.-B. Zheng, H. Deng, Q. Xie, K. Huang, Q. Guo, L. Zhang, P. Zhang, D. Xu, D. Zheng, X. Zhu, H. Wang, Y.-A. Chen, C.-Y. Lu, S. Han, and J.-W. Pan, 10-Qubit Entanglement and Parallel Logic Operations with a Superconducting Circuit, Phys. Rev. Lett. **119**, 180511 (2017).

[81] B. Vlastakis, G. Kirchmair, Z. Leghtas, S. E. Nigg, L. Frunzio, S. M. Girvin, M. Mirrahimi, M. H. Devoret, and R. J. Schoelkopf, Deterministically encoding quantum information using 100-photon Schrödinger cat states, Science **342**, 607 (2013).

[82] A. Omran, H. Levine, A. Keesling, G. Semeghini, T. T. Wang, S. Ebadi, H. Bernien, A. S. Zibrov, H. Pichler, S. Choi, J. Cui, M. Rossignolo, P. Rembold, S. Montangero, T. Calarco, M. Endres, M. Greiner, V. Vuletić, and M. D. Lukin, Generation and manipulation of Schrödinger cat states in Rydberg atom arrays, Science **365**, 570 (2019).

[83] N. Tsuji, M. Eckstein, and P. Werner, Nonthermal Antiferromagnetic Order and Nonequilibrium Criticality in the Hubbard Model, Phys. Rev. Lett. **110**, 136404 (2013).

[84] F. Pollmann, S. Mukerjee, A. G. Green, and J. E. Moore, Dynamics after a sweep through a quantum critical point, Phys. Rev. E **81**, 020101(R) (2010).

[85] E. Canovi, E. Ercolessi, P. Naldesi, L. Taddia, and D. Vodola, Dynamics of entanglement entropy and entanglement spectrum crossing a quantum phase transition, Phys. Rev. B **89**, 104303 (2014).

[86] T. W. B. Kibble, Topology of cosmic domains and strings, J. Phys. A **9**, 1387 (1976).

[87] W. H. Zurek, Cosmological experiments in superfluid helium?, Nature (London) **317**, 505 (1985).

[88] A. Polkovnikov, Universal adiabatic dynamics in the vicinity of a quantum critical point, Phys. Rev. B **72**, 161201(R) (2005).

[89] W. H. Zurek, U. Dorner, and P. Zoller, Dynamics of a Quantum Phase Transition, Phys. Rev. Lett. **95**, 105701 (2005).

[90] J. Dziarmaga, Dynamics of a Quantum Phase Transition: Exact Solution of the Quantum Ising Model, Phys. Rev. Lett. **95**, 245701 (2005).

[91] R. Schützhold, M. Uhlmann, Y. Xu, and U. R. Fischer, Sweeping from the Superfluid to the Mott Phase in the Bose-Hubbard Model, Phys. Rev. Lett. **97**, 200601 (2006).

[92] F. Pellegrini, S. Montangero, G. E. Santoro, and R. Fazio, Adiabatic quenches through an extended quantum critical region, Phys. Rev. B **77**, 140404(R) (2008).

[93] M. Dalmonte, J. Carrasquilla, L. Taddia, E. Ercolessi, and M. Rigol, Gap scaling at Berezinskii-Kosterlitz-Thouless quantum critical points in one-dimensional Hubbard and Heisenberg models, Phys. Rev. B **91**, 165136 (2015).

[94] V. Eisler, Crossover between ballistic and diffusive transport: The quantum exclusion process, J. Stat. Mech. (2011) P06007.

[95] J. Smith, A. Lee, P. Richerme, B. Neyenhuis, P. W. Hess, P. Hauke, M. Heyl, D. A. Huse, and C. Monroe, Many-body localization in a quantum simulator with programmable random disorder, Nat. Phys. **12**, 907 (2016).

[96] R. Costa de Almeida and P. Hauke, From entanglement certification with quench dynamics to multipartite entanglement of interacting fermions, Phys. Rev. Res. **3**, L032051 (2021).

[97] M. Yu, Y. Yang, H. Xiong, and X. Lin, Critical behavior of quantum Fisher information in finite-size open Dicke model, AIP Adv. **12**, 055118 (2022).

[98] W. Zhong, Z. Sun, J. Ma, X. Wang, and F. Nori, Fisher information under decoherence in Bloch representation, Phys. Rev. A **87**, 022337 (2013).

[99] X. Guo, C. R. Breum, J. Borregaard, S. Izumi, M. V. Larsen, T. Gehring, M. Christandl, J. S. Neergaard-Nielsen, and U. L. Andersen, Distributed quantum sensing in a continuous-variable entangled network, Nat. Phys. **16**, 281 (2020).

[100] K. Xu, Y.-R. Zhang, Z.-H. Sun, H. Li, P. Song, Z. Xiang, K. Huang, H. Li, Y.-H. Shi, C.-T. Chen, X. Song, D. Zheng, F. Nori, H. Wang, and H. Fan, Metrological Characterization of Non-Gaussian Entangled States of Superconducting Qubits, Phys. Rev. Lett. **128**, 150501 (2022).

[101] V. Vedral, High-temperature macroscopic entanglement, New J. Phys. **6**, 102 (2004).

[102] H.-C. Jiang, Z. Wang, and L. Balents, Identifying topological order by entanglement entropy, Nat. Phys. **8**, 902 (2012).

[103] A. Szasz, J. Motruk, M. P. Zaletel, and J. E. Moore, Chiral Spin Liquid Phase of the Triangular Lattice Hubbard Model: A Density Matrix Renormalization Group Study, Phys. Rev. X **10**, 021042 (2020).

[104] J. Tindall, F. Schlawin, M. Buzzi, D. Nicoletti, J. R. Coulthard, H. Gao, A. Cavalleri, M. A. Sentef, and D. Jaksch, Dynamical Order and Superconductivity in a Frustrated Many-Body System, Phys. Rev. Lett. **125**, 137001 (2020).